et al., 1996), dopamine D_2 receptors (Kaasinen et al., 2000; Inoue et al., 2001), and dopamine D_1 receptors (Suhara et al., 1991). The results of studies on age-related change of dopamine synthesis have been less consistent, showing decreases (Martin et al., 1989) as well as no changes with aging (Eidelberg et al., 1993; Sawle et al., 1990; Laakso et al., 2001) by PET using 6-[^{18}F]fluoro-L-DOPA. However, previous postmortem studies have reported remarkable age-dependent decreases in the striatal activity of dopa decarboxylase (Lloyd and Hornykiewicz, 1972; Kish et al., 1995). Our study with L-[β-^{11}C]DOPA showed that dopamine synthesis not only in the striatum but also in extrastriatal regions of the living human brain decreased with the normal aging process. 3-*O*-Methyl-L-DOPA, a metabolite of L-DOPA, is known to pass the blood–brain barrier (Wade and Katzman, 1975). In previous PET studies using 6-[^{18}F]fluoro-L-DOPA, dopamine synthesis was affected by 6-[^{18}F]fluoro-3-*O*-methyl-L-DOPA in the brain (Kuwabara et al., 1993; Dhawan et al., 1996). However, nevertheless the 6-[^{18}F]fluoro-3-*O*-methyl-L-DOPA concentrations in the plasma and cerebellum were greater in the elderly group (Kumakura et al., 2005), the time–activity curve of L-[β-^{11}C]DOPA in the occipital, which was used as the reference region did not change with aging in this study. It is also known that 3-*O*-Methylation of 6-fluoro-L-DOPA takes place rapidly as compared to L-DOPA (Torstenson et al., 1999; Melega et al., 1990). The difference between previous results using 6-[^{18}F]fluoro-L-DOPA and ours using L-[β-^{11}C]DOPA may be due to metabolism differences in plasma and brain between the two ligands.

Neutral amino acids are transported from the blood to the brain using the same carrier system in a competitive fashion (Oldendolf, 1971). L-DOPA is also mediated by the same carrier system. K consists of K_1, which represents the influx rate of L-[β-^{11}C]DOPA across the blood–brain barrier, and k_3, which represents the rate of activity of AADC to catabolize L-DOPA to dopamine (Patlak and Blasberg, 1985). L-[β-^{11}C]DOPA is transported in a competitive fashion with neutral amino acids. But it was shown that there was no significant decline in neutral amino acid transport with the carrier system with age (Koeppe et al., 1990; Ito et al., 1995).

K_1 values of L-[β-^{11}C]DOPA were very small (data not shown), indicating that small PS (capillary permeability-

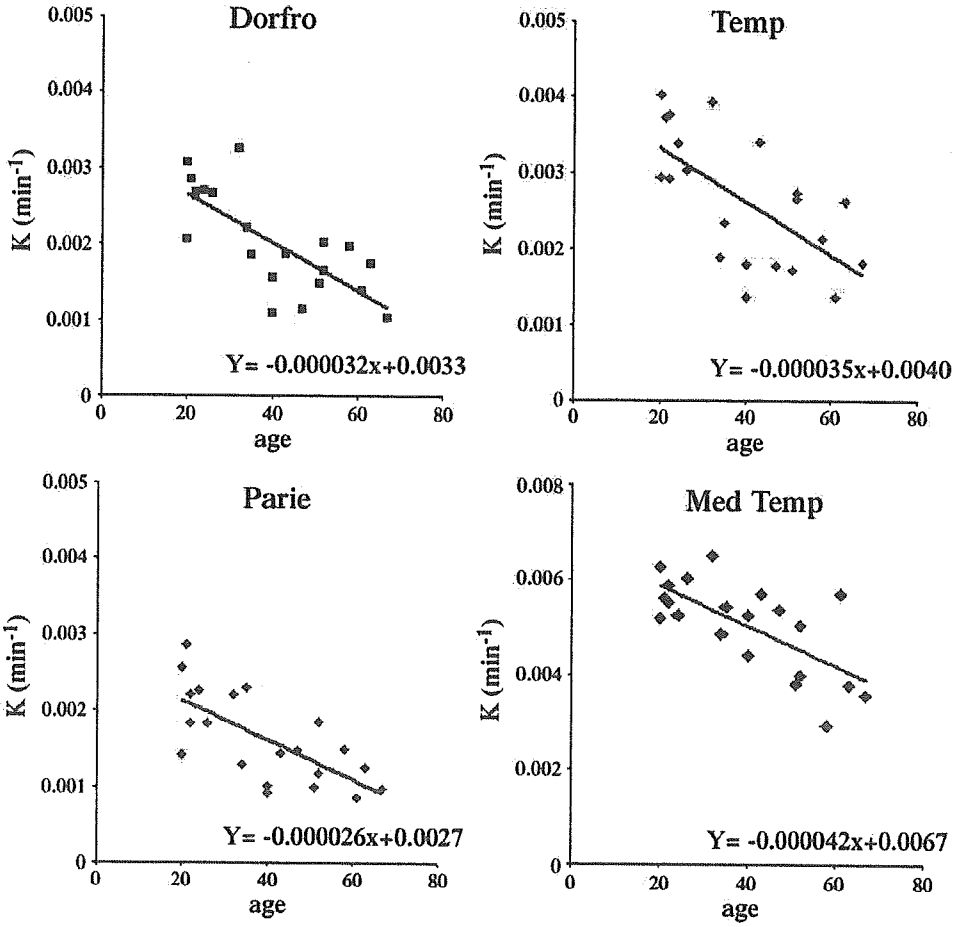

Fig. 1. K of L-[β-^{11}C]DOPA plotted against age in ROI. In the regression equation, 'Y' corresponds to K and 'x' corresponds to age. DorFro, dorsolateral prefrontal cortex; Tempo, lateral temporal cortex; Parie, parietal cortex; Mid, midbrain; Med Tem, medial temporal cortex; ACing, anterior cingulate; Thal, thalamus; Cau, caudate nucleus; Puta, putamen.

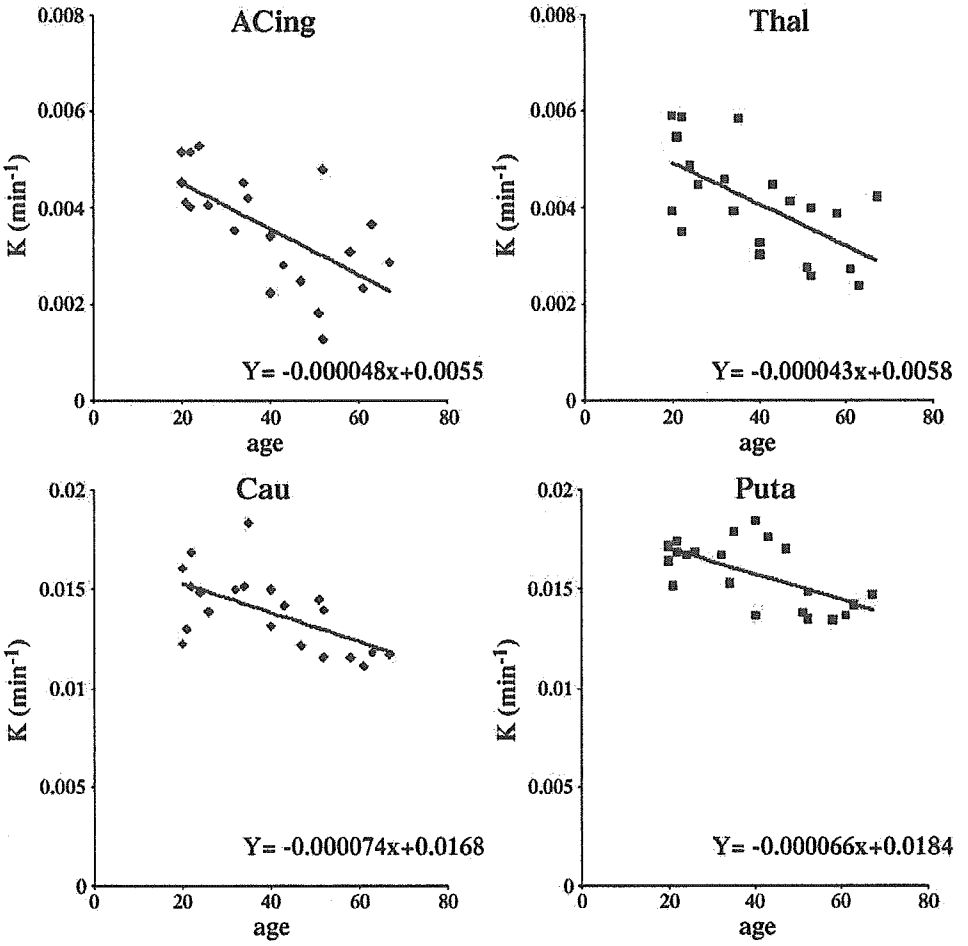

Fig. 1 (*continued*).

surface area product) values, such as K_1 values of L-[β-^{11}C] DOPA, are independent of regional cerebral blood flow (Crone, 1963; Renkin, 1959). With this ligand, graphical analysis using a reference brain region can be used even if the cerebral blood flow changes in a brain region as compared to a reference brain region. Thus, the effect of aging on the K value of L-[β-^{11}C]DOPA must represent the aging effect on dopamine synthesis.

The present study focused on the age-related change in dopamine synthesis. PET studies concerning the aging effect of the striatal dopaminergic neurotransmitter system have shown 6–8% decrease of D_2 receptor binding potential per decade of life (Kaasinen et al., 2000), 6.9% decrease of D_1 receptor binding in the caudate and 7.4% in the putamen per decade (Wang et al., 1998), 8.0% decrease of D_1 receptor binding in the striatum per decade (Suhara et al., 1991), 7.3% decrease of dopamine transporter in caudate nucleus and 5.2% in the putamen per decade (Tupala et al., 2003), and 27% decrease of dopa decarboxylase per 50 years in the postmortem caudate nucleus (Kish et al., 1995). The same magnitude of decline of striatal K was observed in the present study, suggesting a striatal pre- and postsynaptic dopaminergic neurotransmitter system decrease of about 6% per decade. PET studies have also shown a 6% decrease of binding potential of vesicular monoamine transporter, type 2 in the striatum per decade of life (Taylor et al., 2000) and shown the age-related decline in the capacity for [^{18}F] fluorodopamine retention in the striatum (Kumakura et al., 2005). These results were in good agreement with our suggestion. Our study also showed that the rate of dopamine synthesis decline was faster in extrastriatal regions than in the striatum, and especially faster in the dorsolateral prefrontal cortex as compared to the other regions. This result is compatible with the studies of D_1 and D_2 receptors (Suhara et al., 1991; Kaasinen et al., 2000). The dorsolateral

Table 3
Associations of age and tissue fraction of gray matter analyzed using Pearson's correlation coefficients

	Cortex	Med Temp	ACing
Correlation coefficients	−0.777	−0.331	−0.593
p value	0.000	0.142	0.005

Med Temp, medial temporal cortex; ACing, anterior cingulate.

prefrontal cortex is the crucial locus for dopaminergic effects on high-level cognitive functions such as planning, spatial working memory, attention, measure of abstraction, mental flexibility, and verbal fluency (Cools et al., 2002). It is known that the decline in brain dopamine activity contributes to impaired performance of tasks involving the dorsolateral prefrontal regions (Gotham et al., 1988; Owen et al., 1992; Volkow et al., 1998). Our study may suggest that the decline of dopamine synthesis in the dorsolateral prefrontal cortex could explain the decline of cognitive performance with aging. Concerning the lack of aging effect in the midbrain, this region includes the substantia nigra where dopamine is well synthesized. However, the substantia nigra itself is too small in volume to allow accurate quantification of K.

As compared with the aging effects of K, a decline in the tissue fraction of gray matter was found in the cerebral cortex. It is known that volume loss during aging occurs in the cerebral cortex (Taki et al., 2004). Furthermore, areas of relative preservation of gray matter volume were noted symmetrically in the lateral thalami, amygdala, hippocampi, and entorhinal cortex (Good et al., 2001). Our observation is consistent with these results. The degree of decrease in the tissue fraction of gray matter in the cerebral cortical region was smaller than that of the previous report (Taki et al., 2004). This may be due to the fact that the loss of gray matter tissue fraction accelerates through the course of life, and particularly at advanced age, and our subjects were relatively younger than those of the previous study, in which 16–79-year-old subjects participated. In the present study, the decline in cortical K was faster and more diffusely distributed than that of gray matter volume. This may indicate that the dopaminergic function decreases faster than morphological changes.

In this study, we evaluate only in males. Numerous gender-associated functional, biological differences in the dopamine systems of the brain have been described (Kaasinen et al., 2001). Further works concerning sex difference of the dopamine system using the same method will be necessary.

Conclusion

We confirmed the reproducibility of L-[β-^{11}C]DOPA quantification. Significant age-related declines of dopamine synthesis in the striatum and extrastriatal regions were observed, indicating that the previously demonstrated age-related decline in the striatal dopamine synthesis extends to several extrastriatal regions in normal human males. Our results also showed that the rate of dopamine synthesis decline was the same magnitude as the loss of dopamine D_1 and D_2 receptors and transporters.

Acknowledgements

We wish to extend our gratitude to Mr. Katsuyuki Tanimoto, Mr. Akira Ando, Mr. Takahiro Shiraishi, and Mr. Masaru Ohno for operation of the PET scanner, and to Mr. Kazutoshi Suzuki, cyclotron personnel, for synthesizing the radioligand. We also gratefully acknowledge Drs. Jun Kosaka, Yota Fujimura, Akihiro Takano, and Ms Yoshiko Fukushima for their helpful discussions and PET data acquisition. This research was supported by grants from the National Institute of Radiological Sciences.

References

Arranz, B., Blennow, K., Ekman, R., Eriksson, A., Mansson, J.E., Marcusson, J., 1996. Brain monoaminergic and neuropeptidergic variations in human aging. Journal of Neural Transmission 103, 101–115.

Bjurling, P., Watanabe, Y., Oka, S., Nagasawa, T., Yamada, H., Langstrom, B., 1990. Multi-enzymatic syntheses of beta-^{11}C-labeled L-tyrosine and L-DOPA. Acta Chemica Scandinavica 44, 183–188.

Cools, R., Stefanova, E., Barker, R.A., Robbins, T.W., Owen, A.M., 2002. Dopaminergic modulation of high-level cognition in Parkinson's disease: the role of the prefrontal cortex revealed by PET. Brain 125 (Pt 3), 584–594.

Crone, C., 1963. Permeability of capillaries in various organs as determined by use of the indicator diffusion method. Acta Physiologica Scandinavica 58, 292–305.

Dhawan, V., Ishikawa, T., Patlak, C., Chaly, T., Robeson, W., Belakhlef, A., Margouleff, C., Mandel, F., Eidelberg, D., 1996. Combined FDOPA and 3OMFD PET studies in Parkinson's disease. Journal of Nuclear Medicine 37, 209–216.

Eidelberg, D., Takikawa, S., Dhawan, V., Chaly, T., Robeson, W., Dahl, R., Margouleff, D., Moeller, J.R., Patlak, C.S., Fahn, S., 1993. Striatal ^{18}F-DOPA uptake: absence of an aging effect. Journal of Cerebral Blood Flow and Metabolism 13, 881–888.

Fleiss, J., 1986. The Design and Analysis of Clinical Experiments. John Wiley and Sons, New York.

Friston, K.J., Holmes, A.P., Worsley, K.J., Poline, J.B., Frith, C., Frackowiak, R., 1995. Statistical parametric maps in functional imaging: a general linear approach. Human Brain Mapping 2, 189–210.

Gefvert, O., Lindstrom, L.H., Waters, N., Waters, S., Carlsson, A., Tedroff, J., 2003. Different corticostriatal patterns of L-DOPA utilization in patients with untreated schizophrenia and patients treated with classical antipsychotics or clozapine. Scandinavian Journal of Psychology 44 (3), 289–292.

Good, C.D., Johnsrude, I.S., Ashburner, J., Henson, R.N.A., Friston, K.J., Frackowiak, R.S.J., 2001. A voxel-based morphometric study of aging in 465 normal adult human brains. Neuroimage 14, 21–36.

Gotham, A.M., Brown, R.G., Marsden, C.D., 1988. 'Frontal' cognitive function in patients with Parkinson's disease 'on' and 'off' levodopa. Brain 111 (Pt 2), 299–321.

Inoue, M., Suhara, T., Sudo, Y., Okubo, Y., Yasuno, F., Kishimoto, T., Yoshikawa, K., Tanada, S., 2001. Age-related reduction of extrastriatal dopamine D2 receptor measured by PET. Life Sciences 69, 1079–1084.

Ito, H., Hatazawa, J., Murakami, M., Miura, S., Iida, H., Bloomfield, P.M., Kanno, I., Fukuda, H., Uemura, K., 1995. Aging effect on neutral amino acid transport at the blood–brain barrier measured with L-[2-^{18}F]-fluorophenylalanine and PET. Journal of Nuclear Medicine 36, 1232–1237.

Ito, H., Shidahara, M., Inoue, K., Goto, R., Kinomura, S., Taki, Y., Okada, K., Kaneta, T., Sato, K., Sato, T., Fukuda, H., 2005. Effects of tissue heterogeneity on cerebral vascular response to acetazolamide stress measured by an I-123 IMP autoradiographic method with single-photon emission computed tomography. Annals of Nuclear Medicine 19 (4), 251–260.

Kaasinen, V., Vilkman, H., Hietala, J., Nagren, K., Helenius, H., Olsson, H., Farde, L., Rinne, J.O., 2000. Age-related dopamine D2/D3 receptor loss in extrastriatal regions of the human brain. Neurobiology of Aging 21 (5), 683–688.

Kaasinen, V., Nagren, K., Hietala, J., Farde, L., Rinne, J.O., 2001. Sex differences in extrastriatal dopamine d(2)-like receptors in the human brain. American Journal of Psychiatry 158, 308–311.

Kish, S.J., Shannak, K., Rajput, A., 1992. Aging produced a specific pattern of striatal dopamine loss: implication for the etiology of idiopathic Parkinson's disease. Journal of Neurochemistry 58, 642–648.

Kish, S.J., Zhong, X.H., Hornykiewicz, O., Haycock, J.W., 1995. Striatal 3,4-dihydroxyphenylalanine decarboxylase in aging: disparity between post-mortem and positron emission tomography studies? Annals of Neurology 38 (2), 260–264.

Koeppe, R.A., Mangner, T., Betz, A.L., Shulkin, B.L., Allen, R., Kollros, P., Kuhl, D.E., Agranoff, B.W., 1990. Use of [^{11}C]aminocyclohexanecarboxylate for the measurement of amino acid uptake and distribution volume in human brain. Journal of Cerebral Blood Flow and Metabolism 10, 722–739.

Kumakura, Y., Vernaleken, I., Grunder, G., Bartenstein, P., Gjedde, A., Cumming, P., 2005. PET studies of net blood–brain clearance of FDOPA to human brain: age-dependent decline of [^{18}F]fluorodopamine storage capacity. Journal of Cerebral Blood Flow and Metabolism 25, 807–819.

Kuwabara, H., Cumming, P., Reith, J., Leger, G., Diksic, M., Evan, A.C., Gjedde, A., 1993. Human striatal L-dopa decarboxylase activity estimated in vivo using 6-[^{18}F]fluoro-dopa and positron emission tomography: error analysis and application to normal subjects. Journal of Cerebral Blood Flow and Metabolism 13, 43–56.

Laakso, A., Vilkman, H., Bergman, J., Haaparanta, M., Solin, O., Syvalahti, E., Salokangas, R.K.R., Hietala, J., 2001. Sex differences in striatal presynaptic dopamine synthesis capacity in healthy subjects. Biological Psychiatry 52, 759–763.

Lloyd, K.G., Hornykiewicz, O., 1972. Occurrence and distribution of aromatic L-amino acid (L-DOPA) decarboxylase in the human brain. Journal of Neurochemistry 19 (6), 1549–1559.

Mai, J., Assheuer, J., Paxinos, G., 1997. Atlas of the Human Brain. Academic Press, New York.

Markianos, M., Lykouras, L., 1981. Circadian rhythms of dopamine-beta-hydroxylase and c-AMP in plasma of controls and patients with affective disorders. Journal of Neural Transmission 50 (2–4), 149–155.

Martin, W.R.W., Palmer, M.R., Patlak, C.S., Calne, D.B., 1989. Nigrostriatal function in man studies with positron emission tomography. Annals of Neurology 26, 535–542.

Melega, W.P., Luxen, A., Perlmutter, M.M., Nissenson, C.H., Phelps, M.E., Barrio, J.R., 1990. Comparative in vivo metabolism of 6-[^{18}F]fluoro-L-dopa and [^{3}H]L-dopa in rats. Biochemical Pharmacology 39, 1853–1860.

Oldendolf, W.H., 1971. Brain uptake of radiolabeled amino acids, amines, and hexoses after arterial injection. American Journal of Physiology 221, 1629–1639.

Owen, A.M., James, M., Leigh, P.N., Summers, B.A., Marsden, C.D., Quinn, N.P., Lange, K.W., Robbins, T.W., 1992. Fronto-striatal cognitive deficits at different stages of Parkinson's disease. Brain 115 (Pt 6), 1727–1751.

Patlak, C.S., Blasberg, R.G., 1985. Graphical evaluation of blood-to-brain transfer constants from multiple-time uptake data. Generalization. Journal of Cerebral Blood Flow and Metabolism 5, 584–590.

Renkin, E.M., 1959. Transport of potassium-42 from blood to tissue in isolated mammalian skeletal muscles. American Journal of Physiology 197, 1205–1210.

Sasaki, M., Ikemoto, M., Mutoh, M., Haradahira, T., Tanaka, A., Watanabe, Y., Suzuki, K., 2000. Automatic synthesis of L-[β-^{11}C] amino acids using an immobilized enzyme column. Applied Radiation and Isotopes 52 (2), 199–204.

Sawle, G.V., Colebatch, J.G., Shah, A., Brooks, D.J., Marsden, C.D., Frackowiak, R.S.J., 1990. Striatal function in normal aging: implications for Parkinson's disease. Annals of Neurology 28, 799–804.

Suhara, T., Fukuda, H., Inoue, O., Itoh, T., Suzuki, K., Yamasaki, T., Tateno, Y., 1991. Age-related changes in human D1 dopamine receptors measured by positron emission tomography. Psychopharmacology (Berl) 103, 41–45.

Taki, Y., Goto, R., Evans, A., Zijdenbos, A., Neelin, P., Lerch, J., Sato, K., Ono, S., Kinomura, S., Nakagawa, M., Sugiura, M., Watanabe, J., Kawashima, R., Fukuda, H., 2004. Voxel-based morphometry of human brain with age and cerebrovascular risk factors. Neurobiology of Aging 25, 455–463.

Taylor, S.F., Koeppe, R.A., Tandon, R., Zubieta, J.K., Frey, K.A., 2000. In vivo measurement of the vesicular monoamine transporter in schizophrenia. Neuropsychopharmacology 23, 667–675.

Tedroff, J., Aquilonius, S.M., Hartvig, P., Lundqvist, H., Bjurling, P., Langstrom, B., 1992. Estimation of regional cerebral utilization of [^{11}C]-L-3,4-dihydroxy-phenylalanine (DOPA) in the primate by positron emission tomography. Acta Neurologica Scandinavica 85, 166–173.

Torstenson, R., Hartvig, P., Langstrom, B., Westerberg, G., Tedroff, J., 1997. Differential effects of levodopa on dopaminergic function in early and advanced Parkinson's disease. Annals of Neurology 41 (3), 334–340.

Torstenson, R., Tedroff, J., Hartvig, P., Fasth, K.J., Langstrom, B., 1999. A comparison of ^{11}C-labelled L-DOPA and L-fluorodopa as positron emission tomography tracers for the presynaptic dopaminergic system. Journal of Cerebral Blood Flow and Metabolism 19, 1142–1149.

Tupala, E., Hall, H., Bergstrom, K., Mantere, T., Rasanen, P., Sarkioja, T., Hiltunen, J., Tihonen, J., 2003. Different effect of age on dopamine transporters in the dorsal and ventral striatum of controls and alcoholics. Synapse 48, 205–211.

Volkow, N.D., Ding, Y.S., Fowler, J.S., Wang, G.J., Logan, J., Gatley, S.J., Hitzemann, R., Smith, G., Fields, F., Gur, R., Wolf, A.P., 1996. Dopamine transporters decrease with age in healthy subjects. Journal of Nuclear Medicine 37, 554–558.

Volkow, N.D., Gur, R.C., Wang, G.J., Fowler, J.S., Moberg, P.J., Ding, Y.S., Hitzemann, R., Smith, G., Logan, J., 1998. Association between decline in brain dopamine activity with age and cognitive and motor impairment in healthy individuals. American Journal of Psychiatry 155 (3), 344–349.

Wade, L.A., Katzman, R., 1975. 3-O-methyldopa uptake and inhibition of L-DOPA at the blood–brain barrier. Life Sciences 17, 131–136.

Wang, Y., Chan, G.L.Y., Holden, J.E., Dobko, T., Mak, E., Schulzer, M., Huser, J.M., Snow, B.J., Ruth, T.J., Calne, D.B., Stoessl, J., 1998. Age-dependent decline of dopamine D1 receptors in human brain: a PET study. Synapse 30, 56–62.

Available online at www.sciencedirect.com
SCIENCE DIRECT®
Psychiatry Research: Neuroimaging xx (2006) xxx–xxx
PSYCHIATRY RESEARCH NEUROIMAGING
www.elsevier.com/locate/psychresns

An automated method for the extraction of regional data from PET images

Pablo Rusjan[a,*], David Mamo[a,b], Nathalie Ginovart[a,b], Douglas Hussey[a], Irina Vitcu[a], Fumihiko Yasuno[c], Suhara Tetsuya[c], Sylvain Houle[a,b], Shitij Kapur[a,b]

[a]*PET Centre, Centre for Addiction and Mental Health, 250 College Street, Toronto, ON M5T 1R8, Canada*
[b]*Department of Psychiatry, University of Toronto, Canada*
[c]*Brain Imaging Project, National Institute of Radiological Science, Chiba, Japan*

Received 19 September 2005; received in revised form 19 January 2006; accepted 20 January 2006

Abstract

Manual drawing of regions of interest (ROIs) on brain positron emission tomography (PET) images is labour intensive and subject to intra- and inter-individual variations. In order to standardize analysis and improve the reproducibility of PET measures, we have developed an image analysis software for automated quantification of PET data. The method is based on the individualization of a set of standard ROIs using a magnetic resonance (MR) image co-registered with the PET image. In order to evaluate the performance of this automated method, the software-based quantification has been compared with conventional manual quantification of PET images obtained using three different PET radiotracers: [^{11}C]-WAY 100635, [^{11}C]-raclopride and [^{11}C]-DASB. Our results show that binding potential estimates obtained using the automated method highly correlate with those obtained by trained raters using manual delineation of ROIs for frontal and temporal cortex, thalamus, and striatum (global Interclass Correlation Coefficient >0.8). For the three radioligands, the software yields time–activity data that are similar (within 8%) to those obtained by manual quantification, eliminates the investigator-dependent variability, considerably shortens the time required for analysis and thus provides an alternative method for accurate quantification of PET data.

Keywords: PET; Time–activity curves; Brain template; Region of interest; Automated method; Binding potential

1. Introduction

Brain images obtained with positron emission tomography (PET) can be analyzed by two different ways: (a) using voxel-based methods or (b) using region-based methods, the latter method being considered superior for data quantification (Hammers et al., 2002). The goal of region-based analysis is the averaging of radioactivity in an anatomic or functional structure, called region of interest (ROI). Manual techniques for ROI delineation require highly trained personnel and are subject to intra- and inter-operator variations, which can ultimately alter reproducibility of the results. Additionally, the time and labour required for manual delineation of ROIs have been increased with the advent of high resolution PET scanners which can produce hundreds of PET slices. To circumvent these limitations, computer-aided methods have been developed to facilitate and improve the reproducibility of delineation of volumes of

* Corresponding author. Tel: +1 416 535 8501x4215; fax: +1 416 260 4164.
E-mail address: pablo.rusjan@camhpet.ca (P. Rusjan).

0925-4927/$ - see front matter © 2006 Elsevier Ireland Ltd. All rights reserved.
doi:10.1016/j.pscychresns.2006.01.011

interest (VOIs), i.e. set of ROIs describing the single target in a volume space.

Since tracer distribution in PET imaging does not always conform to the simple gray matter/white matter demarcations, or the lobar divisions made on the basis of anatomical divisions (e.g. prefrontal vs. motor cortex) (Evans et al., 1991), direct extraction of ROIs from PET images does not necessarily reflect the ROI's precise anatomical space. While computer vision techniques have been used in some specific situations (Mykkanen et al., 2000; Ohyama et al., 2000; Glatting et al., 2004), indirect determination of ROIs from transformation and registration of atlas-based MR images is the most accepted method to perform region-based analysis of PET images.

Since the earliest work in 1983 (Bajcsy et al., 1983; Bohm et al., 1983), we have seen the development of a number of atlases (Bohm et al., 1991; Greitz et al., 1991; Mazziotta et al., 1995), non-linear image matching techniques (Collins et al., 1995; Thirion, 1998) of one or more atlases (Hammers et al., 2003) as well as multimodal registration techniques (Woods et al., 1998a,b; Ashburner et al., 1997; Hammers et al., 2002; Studholme et al., 1999). Several automatic methods have been presented for delineation of ROIs in MRI images; however most of them have not presented an accurate validation to obtain TAC in PET analysis. Two exceptions are the work presented by Yasuno et al. (2002), which we will discuss in detail in the rest of this work, and the work of Svarer et al. (2005) which attempts to reduce the individual variability applying a warping algorithm to several segmented brains to estimate probabilistic ROIs for an individual brain. Yasuno et al. (2002) developed a technique to fit a standard template of ROIs to an individual brain image assisted by a high-resolution reference magnetic resonance (MR) image. This method utilizes computer vision techniques based on the probabilities of gray matter to refine the transformed ROIs. The major limitations of this method, however, are its restricted applicability to sub-cortical regions (particularly the striatum); the template of ROIs expressed in a non-standard brain and the validation using the area under the curve (AUC) of the time–activity data which may be affected by compensations of excesses and deficiencies of activities.

In the present paper, we address these limitations and present the validation of a novel automated method for time–activity curves (TAC) extraction. First, rather than basing the ROI template on a non-standard space, our approach uses the Montreal Neurological Institute/International Consortium for Brain Mapping (MNI/ICBM) 152 standard brain template, which has the additional benefit of expanding on the number ROIs in the template as well as allowing for a more anatomically valid extension of boundaries pertaining to the respective ROIs. Second, a proper differentiation of gray matter from white matter or cerebrospinal fluid (CSF) is crucial for the accurate delineation of ROIs. This process, also called segmentation, uses a predetermined level of probability of gray matter (threshold). Since the previous method was subject to error particularly for small ROIs, we present a solution that is based on a fitting function empirically found. Third, one of the key features of an automated ROI program is the establishment of boundaries between adjacent ROIs. In the present approach, we created a natural definition of boundary by using multiple iterations of the morphological dilatation that prevents overlap between neighbor ROIs. Finally, we explored the effect of varying the Full-Width at Half-Maximum (FWHM) of the Gaussian smoothing filter and the use of proton density (PD) weighted MR image to improve the segmentation of the subcortical ROIs.

The aim of this work is to present a methodology incorporating these corrections that is applicable to cortical as well as subcortical structures such as the caudate and putamen. Our method is validated for its internal consistency and reliability versus trained human raters using PET radioligands with different patterns of brain radioactivity uptake: [^{11}C]-WAY 100635, which is mainly uptaken in cortical regions, [^{11}C]-raclopride, which is mainly uptaken in the striatum subcortical region, and [^{11}C]-DASB which is uptaken in both cortical and subcortical regions.

2. Materials and methods

Fig. 1 shows a scheme of the method proposed. It consists of the following steps: (1) A standard brain template with a set of predefined ROIs is transformed to match individual high-resolution MR images scan, (2) the ROIs from the transformed template are refined based on the gray matter probability of voxels in the individual MR images, and (3) the individual MR images are co-registered to the PET images so that the individual refined ROIs are transformed to the PET images space. Steps 1 and 3 are executed using the SPM2 (Wellcome Department of Cognitive Neurology, London, UK) algorithms of normalization and co-registration. Different values of cut-off distance and regularizations (smoothness of the deformation fields) are used in the non-linear transformation from the standard brain template to the subject MR images when SPM defaults do not satisfy visual inspection of the transformed image. Nearest neighbor interpolation is used to preserve the codification in the ROIs (described

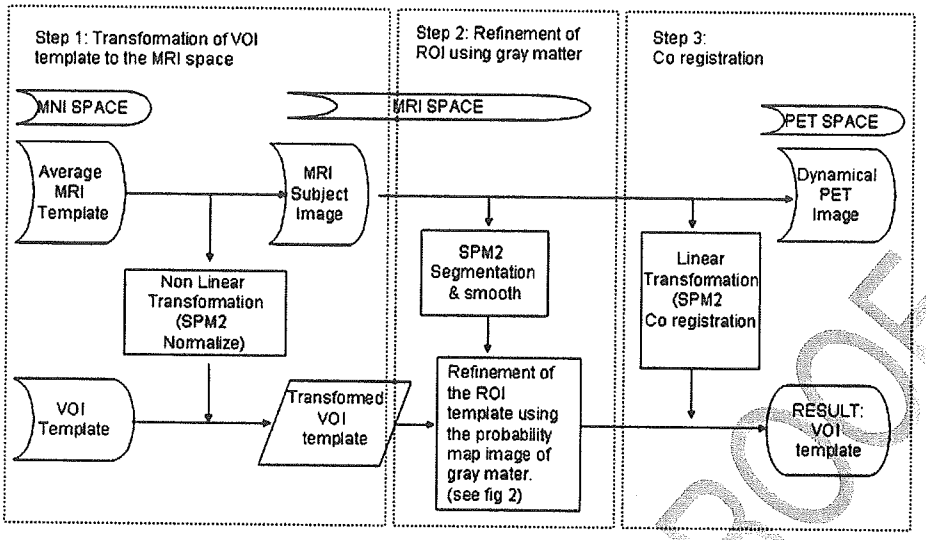

Fig. 1. Flow chart showing the 3 main steps involved in Yasuno's methodology: Step 1: The ROI template in a standard space is transformed to the of MR image space using a non-linear transformation. Step 2: The ROI Template is refined (see Fig. 2) using a probability of gray matter image extracted from the individual MR image. Step 3: The MR image is co-registered to the PET image using Normalized Mutual Information algorithm carrying the ROI template.

below). The multimodal co-registration between the MR and the PET images is done using the normalized mutual information algorithm (Studholme et al., 1999) implemented under SPM2.

The input images are the MR image of the subject (T1 or PD), the dynamic PET image of the subject, a set of ROIs (ROI Template) expressed in a standard brain space, and a MR image (MRI Template) in a standard brain space. The standard brain template chosen was the ICBM/MNI 152 PD brain template smoothed with a kernel of 8 mm that is included in SPM99 as PD.img (http://www.mrc-cbu.cam.ac.uk/Imaging/Common/templates.shtml). This brain volume has a bounding box of −90:91, −126:91, −72:109 sampled at 2-mm intervals with the origin of the coordinate system in the anterior commissure and with the anterior/posterior commissural line as a reference to define the plane where $z=0$ (Talairach and Tournoux, 1988).

The ROI template was created to fit the standard brain image. The Frontal Cortex, Temporal Cortex, Cerebellum, Insula, and Thalamus were taken from the anatomical label atlas of Talairach transformed to standard ICBM/MNI 152 Brain which is included in WFU toolbox (Maldjian et al., 2003) for SPM. Since the anatomical label atlas of Talairach daemon does not distinguish between putamen and nucleus pallidus (referred to as the lentiform nucleus), these two latter subcortical regions were taken from a segmented MNI normalized brain developed by Kabani et al. (1998). In the template, each ROI was codified with a unique number and an additional file was added to the Mayo Clinic Analyze 7.5 Format (www.mayo.edu/bir/PDF/ANALYZE75.pdf) including data on the codification as well as other parameters used in the refinement process.

The goal of the present work was to show reliability of the automated method when compared with manual delineation of ROIs. However, since manual ROI delineation is done on a predetermined number of slices (Bremner et al., 1998), it may not necessarily include all the anatomical structure under study. In this study we limited the number of slices in the template to approximate volumes used by manual raters: cerebellar ROIs were cropped between slices representing planes $z=-48$ and $z=-34$; Putamen, caudate and insula between $z=-6$ and $z=12$ and frontal, thalamus, and temporal between $z=-6$ and $z=16$ in the Talairach coordinate system. (Talairach and Tournoux, 1988).

Since currently available methods for non-linear transformation are inherently imperfect, the transformed ROIs are refined to reflect individual anatomical variations. This refinement step consists of iteratively adding neighboring missing voxels of the ROIs and subsequently removing excess voxels from the ROIs based on the probability of each voxel to belong to the gray matter. In order to do that a gray matter probability map is created with the segmentation algorithm of SPM2 followed by the application of a Gaussian smoothing filter (FWHM=5 mm for [^{11}C]-WAY 100635 and [^{11}C]-DASB; FWHM=1 mm for [^{11}C]-raclopride). For each ROI, a histogram of the probability of each voxel to

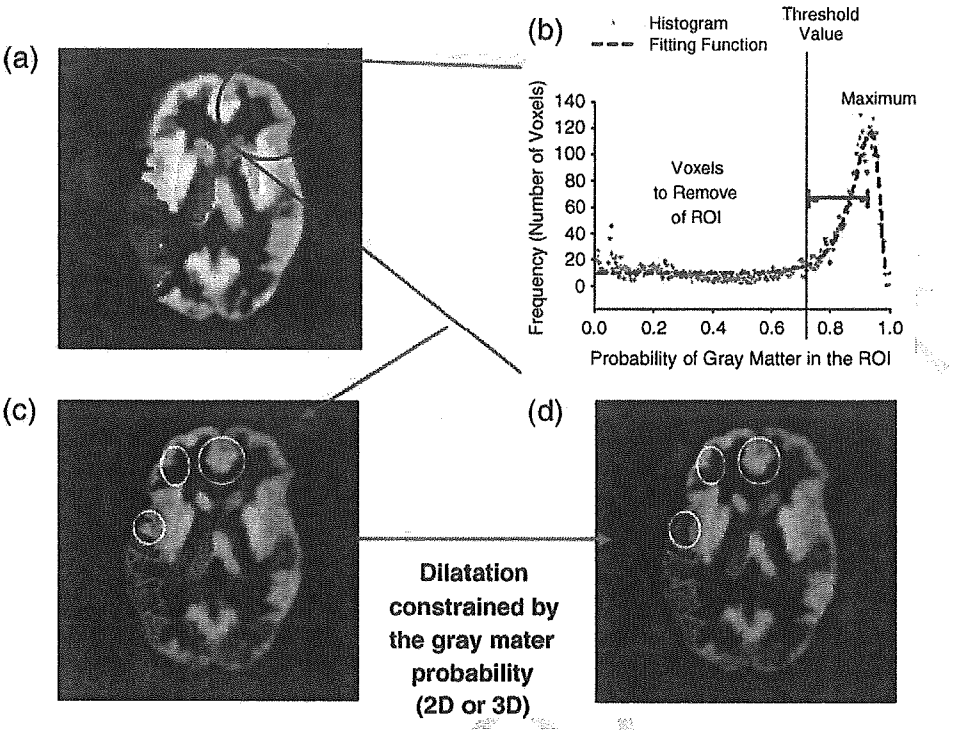

Fig. 2. The refinement step: a) Due to the variability in the inter subject ROIs and characteristics of the methods of normalization the template of ROI is not placed perfectly on the individual brain. b) For each ROI a histogram of values of probability of gray matter is built. The typical shape of this histogram can be fitted by the function shown in Section 2. The maximum of the function is derived analytically. A threshold value of probability is determined as a prefixed fraction of the value which produces the maximum in the histogram. c) Voxels with probability of gray matter in each ROI below the threshold are removed from the ROIs. Secondary to this procedure, the ROI clearly follows the contour of gray matter. d) One iteration of a morphological dilatation is executed. In case of overlap between 2 or more ROIs, overlapped voxels are excluded from all the ROIs. The threshold value of probability is applied again in order to remove dilated voxels on tissue with low probability of gray matter. This dilatation can be applied iteratively.

belong to the gray matter is built. This histogram is fitted with the following function:

$$f(P) = f_0 + a\exp\left[-\frac{1}{2}\left(\frac{\ln\left(\frac{1-P}{1-P_0}\right)}{b}\right)^2\right] \quad (1)$$

where $f(P)$represents the number of voxels with probability of gray matter P within the ROI, and P_0, f_0, b and a are the variables to adjust.

The threshold value of probability of gray matter is determined as a fraction of the value which maximizes the fitting function (P_0). The magnitude of this value is multiplied by 0.85 for the thalamus and 0.90 for all other ROIs. These values are the ones that optimize the results in the work of Yasuno et al. (2002). Voxels in the ROIs corresponding to voxels in MR image with a probability of gray matter lower these thresholds were removed (Fig. 2a and b).

The next step consists in the expansion of the ROIs with the goal of including all voxels that satisfy the threshold of probability and which were excluded in the preceding non-linear transformation. This process is a variation of a morphological dilatation (Serra, 1982) with a kernel ($\begin{smallmatrix}1&1&1\\1&1&1\\1&1&1\end{smallmatrix}$) or its natural extension to 3 dimensions, performed iteratively and constrained to the probability of gray matter above of the threshold (Fig. 2c and d). To prevent overlap of adjacent ROIs during the dilatation process, the following algorithm was applied: in the event of multiple ROIs in the structure element of a voxel, the affected voxel was excluded. The net result of this process when applied iteratively is a natural definition of the boundary of the ROIs. The number of ROIs in the template and the extent of gray matter covered by the ROIs determine the appropriate number of iterations. Results presented in this study were obtained using 2D dilatation due to the highly asymmetrical voxel size of our MR images ($0.86\times0.86\times3$ mm). A single iteration in the refinement step was performed due to the large space between ROIs in the template considered.

The choice of the above parameters was a trade-off between faithfulness to anatomical detail and

susceptibility to partial volume effects. A more conservative ROI is generally less susceptible to partial volume effects and movement during a dynamic scan. Conversely, a less conservative approach might incur significant partial volume effects so that the resulting AUC of the TACs and radioligand binding potential (BP) are lower.

2.1. The software

The method was automated using a software developed de novo by one of the authors (PR). The software runs all the procedures described in the previous section. It also allows for the saving of a tracking file with the parameters, algorithms employed, and results of each procedure. The software was developed in C++ and based on an open source cross-platform graphic user interface (wxWindows) and OpenGL. SPM2 is called in batch mode using the API interface of MATLAB. The software was successfully compiled with GNU C++ compiler under different versions of Window and Linux. The hardware requirements are a video card supporting OpenGL. A copy of the software is available on written request to the principal author.

2.2. Subjects and data acquisition

A total of 28 PET scans previously performed in our PET facilities with three different radiotracers were reused for the purpose of the present study. These scans were performed in healthy control volunteers and were part of independent research protocols. The three radiotracers, [^{11}C]-raclopride, [^{11}C]-DASB and [^{11}C]-WAY 100635, were chosen based on the different brain distribution of their binding: [^{11}C]-raclopride binding to dopamine D_2-receptors was analyzed in putamen and caudate; [^{11}C]-DASB binding to the serotonin transporter was analyzed in thalamus and [^{11}C]-WAY 100635 binding to serotonin 5-HT_{1A} receptors was analyzed in cortical regions.

Nine PET scans were done after bolus injection of 370 MBq of the D_2-receptor radiotracer [^{11}C]-raclopride. Radioactivity in the brain was measured in a series of sequential acquisitions of increasing duration (from 1 to 5 min) for a total duration of 60 min. Ten PET scans were done after bolus injection of 370 MBq of the serotonin transporter radiotracer [^{11}C]-DASB. Radioactivity in the brain was measured in a series of sequential acquisitions of increasing duration (from 1 to 5 min) for a total duration of 90 min. Nine PET scans were done after bolus injection of 370 MBq of the 5-HT_{1A} receptor radiotracer [^{11}C]-WAY 100635. Radioactivity in the brain was measured in a series of sequential acquisitions of increasing duration (from 1 to 5 min) for a total duration of 90 min.

2.3. PET system

Studies were performed on an eight-ring brain PET camera system Scanditronix GE 2048-15B. The Images were corrected for attenuation with a ^{68}Ge transmission scan and were reconstructed using filtered back projection with a Hanning filter 5 mm FWHM. 15 axial slices images, each 6.5 mm thick, were obtained. The intrinsic in-plane resolution of the reconstructed images was 4.5 mm FWHM. The voxel dimensions were 2, 2, and 6.5 mm in x, y, and z axes, with a resolution of $128 \times 128 \times 15$.

2.4. MR images scanning

Each subject underwent magnetic resonance imaging. Spin-echo sequence T1- and proton density-weighted images were obtained on a General Electric medical system (Signa 1.5-T scanner) with x, y, and z voxel dimensions of 0.86, 0.86, and 3.00 mm, respectively, and a matrix of $256 \times 256 \times 43$.

2.5. Manual delineation of ROIs

Each subject's MR image scan was co-registered to the PET scan by using Rview8/mpr realignment software (Studholme et al., 1999).

Regions of interest (ROIs) for the caudate, putamen, thalamus, occipital cortex, frontal cortex and cerebellum were drawn by two independent raters on the co-registered MR images using a commercially available image analysis software (Alice, Hayden Image Processing Group, Perceptive Systems Inc., Boulder, CO, USA). Both raters used the same criteria to delineate ROIs: the gray matter of the cerebellum was drawn on two consecutive slices where the middle cerebellar peduncle was clearly visible, the frontal and temporal cortices were delineated on three axial MR slices in each hemisphere where the striatum was clearly visible, and the putamen, caudate, and thalamus were drawn on two contiguous slices where each one was clearly visible. Regional radioactivity was determined for each frame, corrected for decay, and plotted versus time considering ROIs in each hemisphere independently. Calculation of regional binding potential (BP) values was done using the Simplified Reference Tissue Model (SRTM) (Lammertsma and Hume, 1996) and the kinetic modeling software PMOD V2.4 (PMOD Technologies Ltd., Zurich, Switzerland).

Table 1
Comparison between BPs and TACs obtained with the automated method and by the two manuals raters in the [^{11}C]-WAY 100635 PET studies

	j=Computer k=Rater1	j=Computer k=Rater2	j=Rater2 k=Rater1
Frontal			
%BP(j,k)[a] (mean±S.D.)	5 (±4)	5 (±7)	1 (±5)
ICC BP by pairs	0.96	0.92	0.97
Overlap ratio[b](±S.D.)	0.42 (±.08)	0.36 (±0.06)	
%TAC(j,k)[b] (mean±S.D.)	7 (±1)	5 (±2)	2 (±2)
Temporal			
%BP(j,k)[a] (mean±S.D.)	0 (±7)	0 (±7)	0 (±6)
ICC BP by pairs	0.95	0.93	0.95
Overlap ratio[b] (mean±S.D.)	0.47 (±.09)	0.41 (±0.10)	
%TAC(j,k)[b] (mean±S.D.)	4 (±4)	2 (±3)	1 (±3)
Cerebellum			
Overlap ratio[b] (mean±S.D.)	0.54(±0.19)	0.59(±0.20)	
%TAC(j,k)[b] (mean±S.D.)	3 (±2)	1 (±2)	2 (±4)

[a] %BP(j,k) is the mean (n=9) percentage difference of binding potential (BP) values obtained between methods and was calculated as: 100%×(BP$_j$−BP$_k$)/BP$_k$ with j and k defined in the header of the columns.

[b] Overlap radio, a measure of overlap between ROI, and %TAC(j,k), the percentage difference of time–activity data, were calculated as defined in Section 2.6.

Table 2
Comparison between BPs and TACs obtained with the automated method and by the two manuals raters in the [^{11}C]-raclopride PET studies

	j=Computer k=Rater1	j=Computer k=Rater2	j=Rater2 k=Rater1
Caudate			
%BP(j,k)[a] (mean±S.D.)	4 (±3)	−3 (±8)	7 (±8)
ICC BP by pairs	0.94	0.82	0.76
Overlap ratio[b] (mean±S.D.)	0.48 (±0.15)	0.48 (±0.15)	
%TAC(j,k)[b] (mean±S.D.)	−4 (±5)	−4 (±5)	2(±4)
Putamen			
%BP(j,k)[a] (mean±S.D.)	1 (±6)	−4 (±9)	6 (±4)
ICC BP by pairs	0.86	0.74	0.81
Overlap ratio[b] (mean±S.D.)	0.54 (±.09)	0.54 (±0.10)	
%TAC(j,k)[b] (mean±S.D.)	−4 (±5)	−4 (±5)	1 (±2)
Cerebellum			
Overlap ratio[b] (mean±S.D.)	0.30 (±0.05)	0.53 (±0.13)	
%TAC(j,k)[b] (mean±S.D.)	−6 (±3)	−2 (±2)	−4 (±2)

[a] %BP(j,k) is the mean (n=9) percentage difference of binding potential (BP) values obtained between methods and was calculated as: 100%×(BP$_j$−BP$_k$)/BP$_k$ with j and k defined in the header of the columns.

[b] Overlap radio, a measure of overlap between ROI, and %TAC(j,k), the percentage difference of time–activity data, were calculated as defined in Section 2.6.

Table 3
Comparison between BPs and TACs obtained with the automated method and by the two manuals raters in the [^{11}C]-DASB PET studies

	j=Computer k=Rater1	j=Computer k=Rater2	j=Rater2 k=Rater1
Thalamus			
%BP(j,k)[a] (mean±S.D.)	8 (±15)	2 (±8)	−7 (±12
ICC BP by pairs	0.77	0.90	0.87
Overlap ratio[b] (mean±S.D.)	0.51 (±0.06)	0.63 (±0.05)	
%TAC(j,k)[b] (mean±S.D.)	−8 (±3)	−3 (±2)	−5 (±2)
Cerebellum			
Overlap ratio[b] (mean±S.D.)	0.32 (±0.05)	0.67 (±0.10)	
%TAC(j,k)[b] (mean±S.D.)	−5 (±3)	−3 (±3)	−3 (±1)

[a] %BP(j,k) is the mean (n=10) percentage difference of binding potential (BP) values obtained between methods and was calculated as: 100%×(BP$_j$−BP$_k$)/BP$_k$ with j and k defined in the header of the columns.

[b] Overlap radio, a measure of overlap between ROI, and %TAC(j,k), the percentage difference of time–activity data, were calculated as defined in Section 2.6.

2.6. Validation process

We examined the reliability of the new automated method by comparing BP estimates derived using this method to those derived using manually delineated ROIs as obtained by two independent raters.

The reliability of BP values was determined by means of the intraclass correlation coefficients (ICC) (Lahey et al., 1983; Shrout and Fleiss, 1979):

$$\mathrm{ICC}(1,1) = \frac{\mathrm{BMS}-\mathrm{WMS}}{\mathrm{BMS} + (k-1)\mathrm{WMS}}, \quad (2)$$

where BMS is the mean square between targets, WMS is the within-subject mean square and k is the number of methods or raters. k=2 has been used in the comparison of BP by pairs in Tables 1, 2, and 3, and k=3 has been used in the text in Section 3.2. This coefficient can vary between −1 and +1 where values close to +1 indicate the highest degree of concordance between compared values. We calculated the ICC for BP as it is the main outcome measure used in PET studies.

Since TACs with slightly different profiles may give rise to a similar BP, we also computed in each ROI the ICCs for mean activities as well as the mean percentage difference across subjects between TACs as follows:

$$\%\mathrm{TAC}(j,k) = \sum_{i=1}^{N} (A_j^i - A_k^i)/A_k^i \times 100\% \quad (3)$$

where j and k can be either rater1, rater2 or the computer, N is the total number of data points in the TAC, and A_j^i is the activity value in a given data point i as measured by

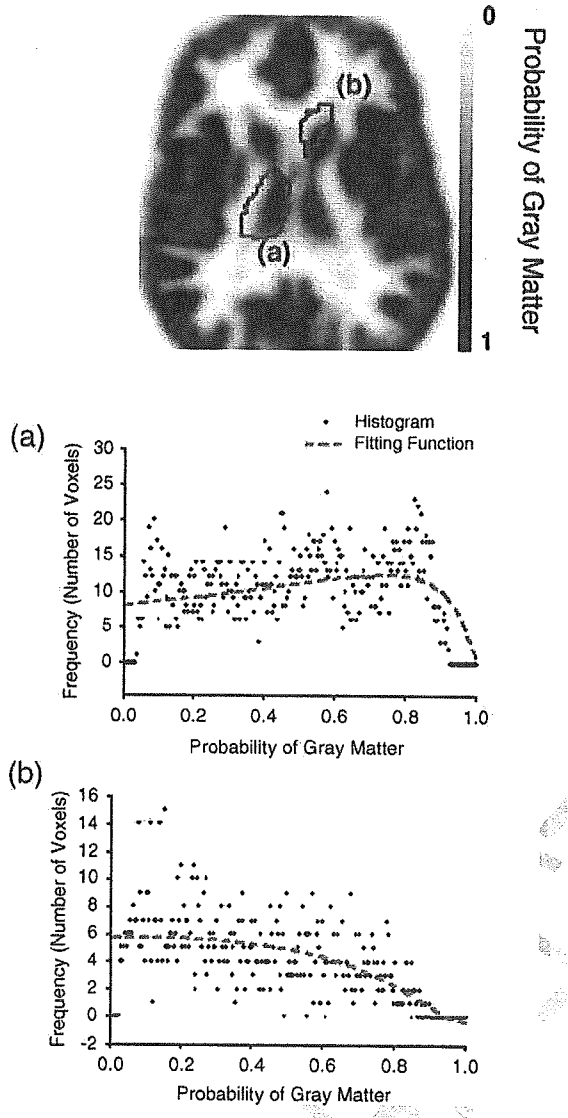

Fig. 3. Two examples in which the fitting function gives robusticity to the method. In the superior section of the figure the transformed left thalamus and right caudate are shown on a 5 mm smooth gray matter probability map. (a) The thalamus falling half inside of the gray matter and half outside shows a histogram of probability of gray matter that presents multiple peaks. The fitting function finds the overall shape of the histogram and gives a precise value for the maximum. (b) The caudate is almost outside of the gray matter so the maximum of the fitting function falls in the negatives values of probability. The solution proposed in this work to this last case in caudate or putamen is using a smooth of 1 mm.

j. An overall positive value of %TAC(j=computer, k=rater1) indicates that activities obtained using the computer (i.e. automated method) are systematically higher than those obtained manually by rater 1 in a given ROI. ROIs were drawn in both hemispheres, but data from the same ROI were pooled to obtain the mean of % TAC(j,k).

In order to get a measure of the overlap between the ROI drawn by the computer and the ROI drawn by the human rater the overlap ratio that was defined as: $(ROI^{computer} \cap ROI^{rater})/(ROI^{computer} \cup ROI^{rater})$ was used. The numerator represents the intersection ROI between computer and human rater, and the dominator represents the union ROI drawn by both. An overlap ratio value of 1 means complete agreement, a value of 0 means no overlap at all, and a overlap of 75% in 2 ROIs of the same size has a overlap ratio 0.6 (Carmichael et al., 2005).

3. Results

3.1. Methodological issues

Yasuno et al. (2002) identified the maximum value of the histogram of probability inside of the ROI and then defined the threshold of probability as a fraction of this peak value. While this procedure may be adequate for large ROIs, the paucity of statistics within a small ROI may result in the occurrence of multiple peaks in the histogram as result of either poor statistics (symbols in Fig. 3a) or shift of the ROI into adjacent CSF or white matter (symbols in Fig. 3b). We defined a fitting function empirically found that clearly characterizes the gray matter (dashed lines in Fig. 3a and b). If the fitting is not successful, the procedure is aborted and a new attempt can be made to improve the parameters used in the non-linear transformation.

Yasuno et al. (2002) applied a 6 mm FWHM smoothing filter on the probability image of gray matter (Fig. 4a). This value was adequate for cortical regions but may be excessive for the striatum due to poor segmentation of the subcortical region, particularly in the border of the insula–putamen. The solution proposed in this work is as follows: for a cortical ROI where gyri and sulci result in a discontinuity in probability of gray matter, a filter of 5 mm (FWHM) is applied, while a smaller filter of 1 mm (FWHM) is more appropriate for more homogenous subcortical ROIs such as the putamen or caudate. The results obtained when applying a 1 mm (FWHM) for segmentation of the striatum are illustrated in Fig. 4b. The procedure allowed a successful separation of right insula–putamen on the right hemisphere but was, as observed in some cases, unsuccessful to resolve it in the left hemisphere.

It is important to note that in this work we have used PD weighted MR images that present a greater contrast in the subcortical areas than T1 weighted MR images resulting in a better segmentation by SPM in these regions.

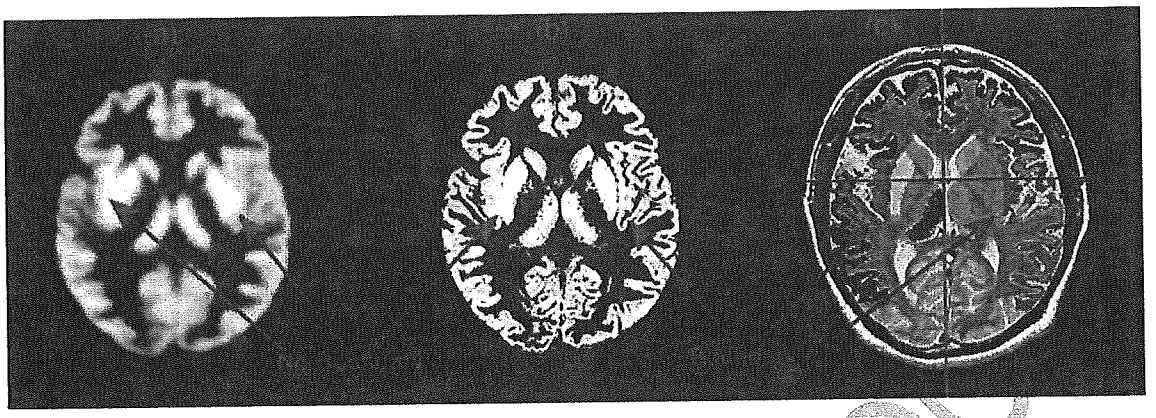

Fig. 4. (a) and (b) show the differences in the striatum–insula boundaries when the probability maps of gray matter when smoothed with a Gaussian filter of FWHM=6 mm and FWHM=1 mm respectively. A large size of the filter completely removes the boundaries (a), a smaller filter (b) is not enough in some cases to see the border. The solution proposed in this work is to add a ROI representing the insula in which to find a border between both ROIs. (c) shows the ROIs on the MR image after 4 iterations of refinement step.

Morphological dilatation of a ROI may result in the overlap of two or more adjacent ROIs. Thus in our method, the growth of an ROI is limited to one voxel in every point of the surface of the ROI during each iteration. Voxels that overlap are not allowed to dilate further. Iterative application of this procedure not only avoids overlap, but also stops unwanted growth of the ROIs. Taking advantage of this property, we have included the insula to create a natural boundary for the putamen. A border automatically appears in images where the map of probability of gray matter does not present a border insula–putamen. This can be seen for the border between the left insula and the left putamen in Fig. 4b and c.

3.2. Validation results

The first step of the validation procedure was to perform a rigorous visual inspection to check concordance between the automated ROIs and the anatomical images as well as the manually drawn ROIs. A global comparison of 92 BPs obtained by two independent raters and with our automated method for 5 ROIs and 3 radiotracers in 28 subjects showed a very good correlation (r=0.96 for each rater; Fig. 5). The linear regression for each rater with respect to the computer shows a straight line near to the identity line (slopes 0.94 and 1.02 and intercepts 0.1 and −0.2 respectively). A detailed comparison of these results is presented in the next three subsections.

3.2.1. Frontal and temporal cortex: studies using [^{11}C]-WAY 100635

The results for nine subjects using [^{11}C]-WAY 100635 in the temporal and frontal ROIs are summarized in Table 1. We found very high correlations between BP values obtained from manual delineation of the ROIs and those obtained using the automated method in both frontal (ICC=0.95) and temporal (ICC=0.94) cortices. The differences between BP values were minimal, being only 5% for the frontal cortex. No difference was observed for BP values obtained in temporal cortex.

Comparison of the TAC data obtained by the manual raters and those obtained by the automated method also demonstrated a very high correlation in both brain structures, with an ICC>0.99. Moreover, the overall difference between TAC data obtained with the automated method and those obtained by the manual raters was positive, thereby indicating that radioactivity concentrations obtained using the automated method were systematically higher than those obtained by the manual

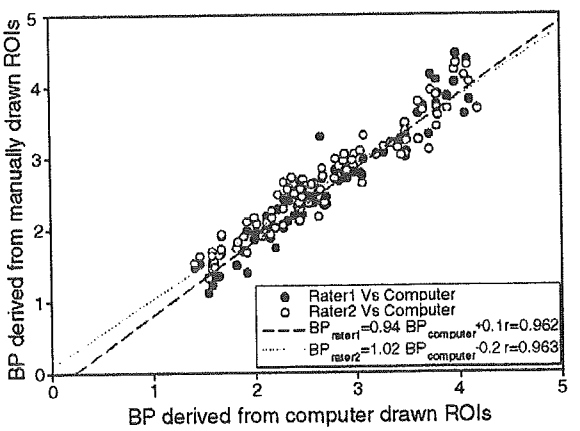

Fig. 5. Comparison of 92 BPs obtained by two independent raters and with our computer software for 5 ROIs and 3 radiotracers in 28 subjects.

raters (Table 1). The overlap ratio between ROIs for frontal and temporal was around 0.4 (see Table 1). A complete visual comparison of the ROIs (not presented here) shows that the automated method was able to carefully delineate the cortices according to its typical sulci, resulting in a more accurate definition of the ROIs than the manually obtained ROI.

3.2.2. Striatum: Studies using [^{11}C]-raclopride

The results for nine subjects using [^{11}C]-raclopride in the caudate and putamen are summarized in Table 2. We found good agreement between automated- and manually derived BPs in the caudate (ICC=0.837) and the putamen (ICC=0.800), with the BP value falling between both raters.

The ICC for all TACs was 0.96. The mean percentage differences between radioactivity levels measured by the computer and the manual raters, %TAC(j=computer, k=manual), were in general negative. The overlap ratio for the caudate was 0.48 and for the putamen was 0.54. Differences in BPs are probably explained by different criteria used by the manual rater to draw the reference ROI (cerebellum). The computer drew similarly as rater 2, including the whole cortex of the cerebellum. Rater 1 drew the cerebellum excluding the vermis. This may explain the somewhat smaller overlap ratio in the cerebellum between the computer and rater 1.

3.2.3. Thalamus: studies using [^{11}C]-DASB

BP values obtained in thalamus using [^{11}C]-DASB are summarized in Table 3. There was a good agreement between BP estimates obtained using the manual and the automated method (ICC=0.819). The BPs generated by the two manual raters were different (mean=7%) and highly variable (S.D.=12%). The computer yielded higher BPs with respect to both raters, with values closer to those generated by rater 2 (2%).

Evaluation of the TACs obtained by the automated and manual methods also showed excellent agreement (ICC for TAC >0.98). Radioactivity concentrations obtained by the manual raters were higher than those obtained by the computer. With respect to rater 2, the differences in cerebellum and thalamus were similar (% TAC(j=computer, k=rater2)=3%). For rater 1, differences for thalamus (%TAC(j=computer, k=rater1)=−8%) were more important than for cerebellum (%TAC (j=computer, k=rater1)=−5%) which explain the larger differences in BPs. The computer drew a thalamus and a cerebellum closer to rater 2 (overlap ratio>.6). A different criteria drawing the cerebellum, as in the previous section, may explain the low overlap ratio (0.32) with rater 1 and the difference in BPs.

4. Discussion

Our principal goal was to develop an automated method to accurately delineate brain ROIs, generate TACs, and derive BP measures of PET radioligands binding. The reliability of the method was tested by comparing TACs and BP measures obtained with this method to those obtained by a conventional manual procedure accomplished by two experienced raters. Our results showed that the automated method yielded fully reproducible TAC and BP data that were highly consistent with those obtained by manual drawing of ROIs. For all TAC obtained, the ICCs were greater than 0.95 and for each ROI the ICC for BP was in the range 0.8–0.95 — suggesting that our method is consistent with the results obtained by well-trained raters. More importantly, any trained rater introduces intra-rater variance as the decision regarding ROI boundaries made in every new attempt. In that respect, the "intra-rater" reproducibility of our automatic method is always 100% due to its automated nature. It means the difference between two or more consecutive automated BP determinations is always 0% while, according to studies performed in our laboratory, the manual intra-rater reproducibility is for example 3% in striatum using [^{11}C]-raclopride (data not shown). Regarding the inter-rater differences, our method could not be distinguished from the manual raters. For the temporal cortex, caudate and putamen, the automated method generally gave an intermediate BP value between those obtained by the two raters. For the frontal cortex and thalamus it gave values generally higher than those obtained by the manual raters. Thus, from all perspectives of inter-rater variance – this method performs quite well – with the added advantage of no intra-rater variance.

The criteria to solve the overlap of two or more adjacent ROIs during the dilatation in the refinement step are an important contribution to the original method. As a result, BPs obtained in putamen were reliable and highly consistent with those estimated by manual rating. This was achieved through the inclusion of the insula as an ROI, which limited the excessive dilatation of the ROI in the putamen. The number of iterations of the dilatation depends on the quantity of ROIs included in the template as well as the volume of gray matter covered by the ROIs. For a limited number of small ROIs (representing a limited fraction of the gray matter volume), excessive iterations will likely lead to ROIs beyond their true anatomical boundaries. Conversely, multiple iterations for large ROIs covering most or all the gray matter will lead to a stable solution. The use of a standard template of ROIs has conferred higher

accuracy for ROI definition through the adoption of accepted standard methodology.

Finally it should be noted that while the procedure described here does not necessarily require any direct intervention from the user, we suggest that some user supervision is required after the non-linear transformation is performed by SPM to ensure a correct global initial position of the ROIs. The time demanded for a single study is around 10 min in a PC Pentium 4, 2.6 GHz, 1 GB RAM.

5. Conclusion

We described a new method for automatic ROI delineation and generation of TACs for brain PET images, improving upon the limitations of previous work by Yasuno et al. (2002). The fitting function of the gray matter probability, the criteria to find borders during the dilatation, the new template expressed in a standard space, and the change in the smoothing of the template confer an excellent stability, increasing the probability of recognizing small ROIs and aborting the process when the non-linear transformation leads to an insurmountable initial conditions. The validation of our method based on the reliability of BP values introduces a most rigorous test for the procedure.

The method only tries to correct inaccuracy on the non-linear transformation. When new image-to-image matching algorithms (Thirion, 1998), geodesics actives contour, and other state of the art algorithms of computer vision are fully automated, validated and freely available for non-rigid registration of MR images, the necessity of such correction will likely decrease. Until that time, this method provides an essential tool for the individualization of the standard atlas using widely accepted software like SPM.

Acknowledgements

We would like to thank Alvina Ng and Anahita Boovariwala for drawing the ROIs, Noor Kabani for the templates of Anatomical Regions of Interest, Jeff Meyer for providing PET data and Laura Acion for statistical help.

References

Ashburner, J., Neelin, P., Collins, D.L., Evans, A., Friston, K., 1997. Incorporating prior knowledge into image registration. Neuroimage 6, 344–352.

Bajcsy, R., Lieberson, R., Reivich, M., 1983. A computerized system for the elastic matching of deformed radiographic images to idealized atlas images. Journal of Computer Assisted Tomography 7, 618–625.

Bohm, C., Greitz, T., Kingsley, D., Berggren, B.M., Olsson, L., 1983. Adjustable computerized stereotaxic brain atlas for transmission and emission tomography. AJNR American Journal of Neuroradiology 4, 731–733.

Bohm, C., Greitz, T., Seitz, R., Eriksson, L., 1991. Specification and selection of regions of interest (ROIs) in a computerized brain atlas. Journal of Cerebral Blood Flow and Metabolism 11, A64–A68.

Bremner, J.D., Bronen, R.A., De Erasquin, G., Vermetten, E., Staib, L.H., Ng, C.K., Soufer, R., Charney, D.S., Innis, R.B., 1998. Development and reliability of a method for using magnetic resonance imaging for the definition of regions of interest for positron emission tomography. Clinical Positron Imaging 1, 145–159.

Carmichael, O.T., Aizenstein, H.A., Davis, S.W., Becker, J.T., Thompson, P.M., Meltzer, C.C., Liu, Y., 2005. Atlas-based hippocampus segmentation in Alzheimer's disease and mild cognitive impairment. Neuroimage 27, 979–990.

Collins, D.L., Holmes, C.J., Peters, T.M., Evans, A., 1995. Automatic 3-d model-based neuroanatomical segmentation. Human Brain Mapping 3, 190–208.

Evans, A.C., Marrett, S., Torrescorzo, J., Ku, S., Collins, L., 1991. MRI–PET correlation in three dimensions using a volume-of-interest (VOI) atlas. Journal of Cerebral Blood Flow and Metabolism 11, A69–A78.

Glatting, G., Mottaghy, F.M., Karitzky, J., Baune, A., Sommer, F.T., Landwehrmeyer, G.B., Reske, S.N., 2004. Improving binding potential analysis in [^{11}C]raclopride PET studies using cluster analysis. Medical Physics 31, 902–906.

Greitz, T., Bohm, C., Holte, S., Eriksson, L., 1991. A computerized brain atlas: construction, anatomical content, and some applications. Journal of Computer Assisted Tomography 15, 26–38.

Hammers, A., Koepp, M.J., Free, S.L., Brett, M., Richardson, M.P., Labbe, C., Cunningham, V.J., Brooks, D.J., Duncan, J., 2002. Implementation and application of a brain template for multiple volumes of interest. Human Brain Mapping 15, 165–174.

Hammers, A., Allom, R., Koepp, M.J., Free, S.L., Myers, R., Lemieux, L., Mitchell, T.N., Brooks, D.J., Duncan, J.S., 2003. Three-dimensional maximum probability atlas of the human brain, with particular reference to the temporal lobe. Human Brain Mapping 19, 224–247.

Kabani, N.J., MacDonald, D., Holmes, C.J., Evans, A.C., 1998. 3D anatomical atlas of the human brain. Neuroimage 7, S717.

Lahey, M.A., Downey, R.G., Saal, F.E., 1983. Intraclass correlations: there's more there than meets the eye. Psychological Bulletin 93, 586–595.

Lammertsma, A.A., Hume, S.P., 1996. Simplified reference tissue model for PET receptor studies. Neuroimage 4, 153–158.

Maldjian, J.A., Laurienti, P.J., Kraft, R.A., Burdette, J.H., 2003. An automated method for neuroanatomic and cytoarchitectonic atlas-based interrogation of fMRI data sets. Neuroimage 19, 1233–1239.

Mazziotta, J.C., Toga, A.W., Evans, A., Fox, P., Lancaster, J., 1995. A probabilistic atlas of the human brain: theory and rationale for its development. The International Consortium for Brain Mapping (ICBM). Neuroimage 2, 89–101.

Mykkanen, J.M., Juhola, M., Ruotsalainen, U., 2000. Extracting VOIs from brain PET images. International Journal of Medical Informatics 58–59, 51–57.

Ohyama, M., Senda, M., Mishina, M., Kitamura, S., Tanizaki, N., Ishii, K., Katayama, Y., 2000. Semi-automatic ROI placement

system for analysis of brain PET images based on elastic model: application to diagnosis of Alzheimer's disease. The Keio Journal of Medicine 49 (Suppl 1), A105–A106.

Serra, J.P., 1982. Image Analysis and Mathematical Morphology. Academic Press, London; New York.

Shrout, P.E., Fleiss, J.L., 1979. Intraclass correlations: uses in assessing rater reliability. Psychological Bulletin 86, 420–428.

Studholme, C., Hill, D.L.G., Hawkes, D.J., 1999. An overlap invariant entropy measure of 3D medical image alignment. Pattern Recognition 32, 71–86.

Svarer, C., Madsen, K., Hasselbalch, S.G., Pinborg, L.H., Haugbol, S., Frokjaer, V.G., Holm, S., Paulson, O.B., Knudsen, G.M., 2005. MR-based automatic delineation of volumes of interest in human brain PET images using probability maps. Neuroimage 24, 969–979.

Talairach, J., Tournoux, P., 1988. Co-Planar Stereotaxic Atlas of the Human Brain: 3-Dimensional Proportional System: an Approach to Medical Cerebral Imaging. G. Thieme, Stuttgart.

Thirion, J.P., 1998. Image matching as a diffusion process: an analogy with Maxwell's demons. Medical Image Analysis 2, 243–260.

Woods, R.P., Grafton, S.T., Holmes, C.J., Cherry, S.R., Mazziotta, J.C., 1998a. Automated image registration: I. General methods and intrasubject, intramodality validation. Journal of Computer Assisted Tomography 22, 139–152.

Woods, R.P., Grafton, S.T., Watson, J.D., Sicotte, N.L., Mazziotta, J.C., 1998b. Automated image registration: II. Intersubject validation of linear and nonlinear models. Journal of Computer Assisted Tomography 22, 153–165.

Yasuno, F., Hasnine, A.H., Suhara, T., Ichimiya, T., Sudo, Y., Inoue, M., Takano, A., Ou, T., Ando, T., Toyama, H., 2002. Template-based method for multiple volumes of interest of human brain PET images. Neuroimage 16, 577–586.

Epilepsia, **46**(Suppl. 1):11–14, 2005
Blackwell Publishing, Inc.

Symposium I

Intellectual Disability and Psychotic Disorders of Adult Epilepsy

*Masato Matsuura, †Naoto Adachi, ‡Reimi Muramatsu, ‡Masaaki Kato, ‡Teiichi Onuma, §Yoshiro Okubo, ||Yasunori Oana, and ¶Tsunekatsu Hara

**Department of Neuropsychiatry, Nihon University School of Medicine, Tokyo; †Adachi Mental Clinic, Sapporo; ‡National Center for Neurology and Psychiatry, §Tokyo Medical and Dental University, ||Saint Paul Hospital, and ¶Komagino Hospital, Tokyo, Japan*

Summary: *Purpose:* To investigate the prevalence, psychopathology, and cognitive functions associated with psychotic disorders among adult epilepsy patients with intellectual disability (ID) based on a multicenter study in Japan.

Methods: The study was divided into three phases; a prevalence study of psychotic disorders among new referrals of epilepsy, a polydiagnostic comparative study of patients with psychotic epilepsy and those with schizophrenia, and a neuropsychological study of patients with psychotic epilepsy and education level–matched controls.

Results: Among 336 new referrals of epilepsy, a higher prevalence of psychotic disorders was found among patients with ID (24%) than among those with normal intelligence (6%). The psychotic symptoms and operational diagnoses of psychotic epilepsy patients with ID were similar to those of patients with normal intelligence. A wide range (7–86%) of psychotic epilepsy patients was diagnosed as having schizophrenia, depending on the operational criteria used. Patients with psychotic epilepsy had more disturbances in verbal memory and attention functions than did the controls.

Conclusions: Epilepsy patients with ID show a predisposition to develop psychotic disorders. Distinguishing their psychotic symptoms from those of schizophrenia is difficult. Subtle cognitive disturbances predispose to psychotic disorders in epilepsy. **Key Words:** Epilepsy—Intellectual disability—Psychotic disorder—Polydiagnosis—Symptomatology—Neuropsychology.

Many previous studies have reported that epilepsy patients with intellectual disability (ID) are liable to develop all types of psychiatric disorders, including psychotic disorders (1–4). Most clinicians believe that psychotic patients with ID lack the usual richness of the symptoms because of their inability to conceptualize their feelings and describe them to others, as well as an impoverished life experience. Psychotic symptoms are believed to be florid but banal, and to dominate delusions and hallucinations that reflect the naïve and wishful thinking, bizarre, impulsive, aggressive, and unpredictable behaviors. However, no evidence exists that the nature of the psychotic disorders in individuals with ID differs from those without (5). The prevalence, psychopathology, and association with cognitive dysfunction of psychiatric disorders among adult patients with epilepsy and ID require further clarification.

Address correspondence and reprint requests to Dr. M. Matsuura at Section of Biofunctional Information, Graduate School of Allied Health Sciences, Tokyo Medical and Dental University, 1-5-45 Yushima, Bunkyo-ku, Tokyo 113-8519, Japan. E-mail: matsu.mtec@tmd.ac.jp

SUBJECTS AND METHODS

We conducted a three-phase study on this issue. The first phase assessed the prevalence of psychotic disorders among new referrals of adult epilepsy by using a newly developed multiaxial classification scheme (6) based on a multicenter study in Japan (1). Next, we compared the symptoms and operational diagnoses between psychotic disorders in epilepsy and age- and sex-matched schizophrenia patients diagnosed with ICD-10 criteria by using the Japanese version of Operational Criteria Checklist for Psychotic Illness (J-OPCRIT) system (7). Finally, we compared the cognitive function among psychiatric disorders in epilepsy and age-, sex-, and education level–matched controls of epilepsy patients without psychiatric disorders and those with schizophrenia, by using a standardized neuropsychological test battery.

Exclusion criteria were the presence of severe ID with a lack of ability to communicate, alteration of consciousness during psychoses, personal history of alcohol abuse, and severe head trauma after the onset of epilepsy. Group differences were statistically analyzed by using χ^2 tests with Fisher's exact probability tests for nonparametric data and

TABLE 1. *Prevalence of psychotic disorders among new referrals with epilepsy*

	Epilepsy without ID	Epilepsy with ID	Group difference
Number of cases (male/female)	260 (130/130)	38 (21/17)	
Age (yr)	33.1 ± 12.2	27.8 ± 9.8	*a*
Age at onset of epilepsy (yr)	18.5 ± 12.9	12.1 ± 10.8	*b*
Type of epilepsy: PE/GE	74/25%	79/18%	*a*
Seizure frequency: free/yearly/monthly	8/48/44%	13/36/51%	*a*
Presence of epileptic discharges on EEG	66%	69%	NS
Presence of abnormal slow background EEG	38%	64%	*b*
Presence of history of brain damage	18%	59%	*b*
Presence of abnormal findings by CT/MRI	22%	48%	*b*
Presence of psychiatric disorders (ICD-10 category)	23%	66%	*b*
Organic mental disorders (F0)	1	5	*a*
Substance use disorders (F1)	1	0	NS
Psychotic disorders (F2)	6	24	*b*
Mood disorders (F3)	2	3	NS
Neurotic disorders (F4)	7	13	NS
Personality disorders (F6)	5	21	*b*

ID, Intellectual disability; PE/GE, partial epilepsy/generalized epilepsy; NS, not significant.
$^{a}p < 0.05$; $^{b}p < 0.01$ (χ^2 test/ ANOVA).

by using analysis of variance (ANOVA) and post hoc multiple comparisons by Fisher's PLSD for parametric data.

RESULTS

Prevalence of psychotic disorders among new referrals with epilepsy

Two hundred ninety-eight adult patients with epilepsy were included in the first phase of the study (Table 1). The organic feature was dominant among the epilepsy patients with ID compared with those without ID, reflected by higher frequencies of slow EEG activity, history of brain damage, and abnormal computed tomography (CT)/magnetic resonance imaging (MRI) findings. The prevalence of psychiatric and psychotic disorders was significantly higher in the epilepsy with ID group than in the without-ID group. The most prevalent psychiatric disorders were neurotic disorders (7%) in the without-ID group and psychotic disorders (24%) in the with-ID group. The second most prevalent disorders were psychotic disorders in the without-ID group (6%) and personality disorders (21%) in the with-ID group.

Clinical symptoms and operational diagnoses of epilepsy with a psychotic disorder and schizophrenia

Compared with the control group (56 patients with schizophrenia), the psychotic epilepsy groups (51 epilepsy patients without ID and 28 epilepsy patients with ID) were characterized by significantly lower frequencies of a family history of schizophrenia and deterioration of function from premorbid level, and higher ratios of abrupt onset of psychosis and remission (Table 2). The response rate of psychotic symptoms to neuroleptics was similar among all groups.

Psychotic symptoms were similar between the psychotic epilepsy groups without ID and with ID, characterized by a significantly higher frequency of accompanying affective symptoms and lower frequencies of negative and positive symptoms compared with those of the schizophrenia group. The operational diagnoses also were similar between the two psychotic epilepsy groups, and the schizophrenia diagnosis of them ranged from 7% to 68%, depending on the operational criteria used. Schneider's schizophrenia with first-rank symptoms was present to a similar degree in both of the psychotic epilepsy groups. Other prevalent diagnoses of the psychotic epilepsy were atypical psychosis by *Diagnostic and Statistical Manual of Mental Disorders–III* (DSM-III) or psychotic disorder not otherwise specified by DSM-IV.

Neuropsychological profiles of epilepsy with and without psychotic disorder and schizophrenia

Twenty-two psychotic epilepsy patients, 22 epilepsy patients without a psychiatric disorder, and 16 schizophrenia patients were enrolled in the neuropsychological study (Table 3). Wechsler Adult Intelligence Scale (WAIS)-R full-scale IQ, verbal IQ, and comprehension subscore were significantly lower in the psychotic epilepsy group than in the other two groups. Wechsler Memory Scale (WMS) memory quotient and nonrelated paired associate subscore, and WAIS-R digit symbol and picture-arrangement subscores were significantly lower in the psychotic epilepsy group than in the epilepsy group without a psychiatric disorder. WAIS-R similarity and digit span subscores were significantly lower in the psychotic epilepsy group than in the schizophrenia group. WAIS-R performance IQ and WCST category number did not differ among the three groups.

TABLE 2. *Symptoms and operational diagnoses of schizophrenia and epilepsy with a psychotic disorder*

Group	Schizophrenia	Epilepsy without ID	Epilepsywith ID	Group difference
Number of cases (male/female)	56 (26/30)	51 (24/27)	28 (18/10)	
Age (yr)	38.5 ± 11.8	35.0 ± 11.4	38.1 ± 16.6	NS
Age at onset of epilepsy (yr)	–	13.1 ± 7.8	12.3 ± 13.4	NS
Age at onset of psychosis (yr)	25.0 ± 9.9	28.0 ± 10.1	29.6 ± 12.6	NS
Family history of schizophrenia	27%	4%	7%	*a*
Mode of onset: abrupt/acute/gradual	16/23/60%	40/27/40%	43/25/36%	*b*
Course: remission/recurrent/chronic	18/36/47%	54/10/35%	50/14/36%a	*a*
Deterioration from premorbid function	66%	22%	21%	*a*
Response to neuroleptics	73%	75%	57%	NS
Clinical symptoms				
Lack of insight	88%	65%	71%	*b*
Delusions/hallucinations last for 1 wk	73	43	61	*a*
Loss of energy	68	29	11	*a*
Blunted affect	57	18	11	*a*
Slowed activity	55	25	18	*a*
Restricted affect	55	20	14	*a*
Primary delusional perception	50	10	18	*a*
Bizarre behavior	48	65	64	*b*
Abusive/accusatory/persecutory voices	43	14	14	*a*
Well-organized delusions	38	6	11	*a*
Negative formal thought disorder	36	16	7	*a*
Third-person auditory hallucinations	36	8	0	*a*
Delusions of passivity	23	8	4	*b*
Positive formal thought disorder	16	6	0	*b*
Accompanying affective symptoms	14	41	25	*b*
Diminished libido	13	2	0	*b*
Operational diagnosis of schizophrenia				
ICD-10 schizophrenia	100%	49%	50%	*a*
Taylor & Abrahams' schizophrenia	96	49	57	*a*
RDC schizophrenia	85	43	68	*a*
Carpenter's schizophrenia	72	68	50	NS
Schneider's schizophrenia	71	37	39	*a*
DSM-III-R schizophrenia	70	27	25	*a*
DSM-IV schizophrenia	63	18	21	*a*
DSM-III schizophrenia	63	16	14	*a*
French chronic schizophrenia	57	14	7	*a*
St. Louis' schizophrenia	55	18	7	*a*

ID, Intellectual disability; NS, not significant.
$^{a}p < 0.01$; $^{b}p < 0.05$ (χ^2 test/analysis of variance).

DISCUSSION

The present study confirmed that the presence of ID, which may stem from organic brain dysfunction, in epilepsy patients is a risk factor for developing a psychotic disorder. However, psychotic symptoms and psychiatric diagnoses were similar in epilepsy patients with ID and those without ID. Among the general population with ID, the similarities in psychopathology between patients with normal intelligence and those with mild ID have already been documented (8). Although patients with psychotic epilepsy showed lower frequencies of negative and positive symptoms than did schizophrenic patients, a significant number of them were diagnosed as having schizophrenia. The presence of nuclear schizophrenia symptoms are in line with previous reports on psychotic epilepsy patients without ID (9–11) as well as those with ID (12). Although some previous reports pointed out that a low IQ is a risk factor for a chronic course of psychoses in epilepsy (13,14), the present results suggest that the prognosis of epileptic psychosis is better than that of schizophrenia. The discrepancy may be due to the exclusion of severe ID patients in the present study.

The attention and verbal factors revealed by WAIS-R (15), as well as verbal memory detected by WMS, were poorer in the psychotic epilepsy patients than in the controls. These results support the hypothesis that psychotic disorders in epilepsy are associated with underlying cognitive defects (11,14,16). Mellers et al. (17) reported that epilepsy patients with schizophrenia-like psychosis showed a global cognitive dysfunction comparable to that of schizophrenia. Caplan et al. (18) hypothesized that illogical thinking stemming from global cognitive dysfunction in epilepsy contributes to the development of schizophrenia-like psychosis. Verbal dysfunction and attentional deficits, which may result in a reduced capacity to deal with complex social problems, may predispose to psychotic disorders in epilepsy.

TABLE 3. *Neuropsychological profiles of schizophrenia and epilepsy with and without psychotic disorder*

	Schizophrenia	Epilepsy with a psychotic disorder	Epilepsy without a psychiatric disorder	Group difference
Number of cases (male/female)	16 (9/7)	22 (17/5)	22 (14/8)	NS
Age (yr)	36.9 ± 10.4	37.2 ± 8.4	36.0 ± 9.3	NS
Education (yr)	13.6 ± 2.1	13.6 ± 2.2	13.9 ± 2.1	NS
Age at onset of epilepsy (yr)	–	11.2 ± 6.7	16.0 ± 11.9	NS
Age at onset of psychosis (yr)	24.0 ± 10.2	25.4 ± 4.1	–	NS
WAIS-R full-scale IQ	84.0 ± 18.4	75.6 ± 18.5	86.5 ± 14.4	[a]
Verbal IQ	86.3 ± 16.5	76.9 ± 17.4	86.4 ± 11.0	[a]
Performance IQ	84.5 ± 17.9	79.2 ± 19.1	89.4 ± 11.0	NS
Comprehension	7.1 ± 3.1	5.5 ± 2.7	7.1 ± 3.1	[a]
Similarity	7.6 ± 3.6	5.9 ± 4.0	7.1 ± 3.7	[a]
Digit span	8.6 ± 2.6	7.1 ± 2.5	7.5 ± 2.3	[a]
Digit symbol	7.0 ± 3.1	5.2 ± 3.5	7.5 ± 2.5	[a]
Picture arrangement	7.9 ± 2.8	6.4 ± 4.1	9.0 ± 3.1	[a]
WMS				
Memory quotient	90.0 ± 20.3	84.1 ± 15.7	91.7 ± 14.5	[a]
Nonrelated paired associate	4.8 ± 4.1	3.6 ± 3.5	5.6 ± 3.6	[a]
WCST category number	3.6 ± 2.2	3.5 ± 2.3	3.6 ± 2.5	NS

NS, not significant; WAIS-R, Wechsler Adult Intelligence Scale–Revised; WMS, Wechsler Memory Scale; WCST, Wisconsin Card Sorting Test.
[a] $p < 0.05$ (χ^2 test/analysis of variance).

REFERENCES

1. Matsuura M, Oana Y, Kato M, et al. A multi-center study on the prevalence of psychiatric disorders among new referrals for epilepsy in Japan. *Epilepsia* 2003;44:107–14.
2. Devinsky O. What do you do when they grow up? Approaches to seizures in developmentally delayed adults. *Epilepsia* 2002;43(suppl 3):71–9.
3. Adachi N, Matsuura M, Okubo Y, et al. Predictive variables of interictal psychosis in epilepsy. *Neurology* 2000;55:1310–4.
4. Lund J. The prevalence of psychiatric morbidity in mentally retarded adults. *Acta Psychiatr Scand* 1985;72:563–70.
5. American Psychiatric Association. *Diagnostic and statistical manual of mental disorders*. 4th ed, rev. Washington, DC: American Psychiatric Press, 1994.
6. Matsuura M, Adachi N, Oana Y, et al. A proposal for a new five-axial classification scheme for psychoses of epilepsy. *Epilepsy Behav* 2000;1:343–52.
7. Matsuura M, Adachi N, Oana Y, et al. A polydiagnostic and dimensional comparison of epileptic psychoses and schizophrenia spectrum disorders. *Schizophrenia Res* 2004;69:189–201.
8. World Health Organization. *ICD-10 guide for mental retardation*. Geneva: World Health Organization, 1996.
9. Toone BK, Garralda ME, Ron MA. The psychoses of epilepsy and the functional psychoses. *Br J Psychiatry* 1980;137:245–9.
10. Perez MM, Trimble MR, Murray NMF, et al. Epileptic psychosis: an evaluation of PSE profiles. *Br J Psychiatry* 1985;146:155–63.
11. Oyebode F, Davison K. Epileptic schizophrenia: clinical features and outcome. *Acta Psychiatr Scand* 1989;79:327–31.
12. Kanemoto K, Tsuji T, Kawasaki J. Reexamination of iterictal psychoses based on DSM IV psychosis classification and international epilepsy classification. *Epilepsia* 2001;42:98–103.
13. Kristensen O, Sindrup EH. Psychomotor epilepsy and psychosis, III: social and psychological correlates. *Acta Neurol Scand* 1979;59:1–9.
14. Umbricht D, Degreef G, Barr WB, et al. Postictal and chronic psychoses in patients with temporal lobe epilepsy. *Am J Psychiatry* 1995;152:224–31.
15. Kaufman AS. *Assessing adolescent and adult intelligence*. Boston, Mass: Allyn & Bacon, 1990.
16. Ferguson SM, Rayport M, Gardner R, et al. Similarities in mental content of psychotic state, spontaneous seizures, dreams and responses to electrical brain stimulation in patients with temporal lobe epilepsy. *Psychosom Med* 1969;31:479–98.
17. Mellers JDC, Toone BK, Lishman WA. A neuropsychological comparison of schizophrenia and schizophrenia-like psychosis of epilepsy. *Psychol Med* 2000;30:325–35.
18. Caplan R, Arbelle S, Guthrie D, et al. Formal thought disorder and psychopathology in pediatric primary generalized and complex partial epilepsy. *J Am Acad Child Adolesc Psychiatry* 1997;36:1286–94.

Correlation Between Quantitative-EEG Alterations and Age in Patients With Interferon-α–Treated Hepatitis C

Satoshi Kamei, Kentaro Oga,† Masato Matsuura,‡ Naohide Tanaka,§ Takuya Kojima,‡ Yasuyuki Arakawa,§ Yoshihiro Matsukawa,‖ Tomohiko Mizutani,* Teiichiro Sakai,‡ Hitoshi Ohkubo,¶ Hiroshi Matsumura,† Mitsuhiko Moriyama,§ and Kaname Hirayanagi#*

Abstract: The authors recently observed alterations in the quantitative EEG findings in patients with chronic hepatitis C who were treated with interferon-α (IFN-α). However, the factors that influenced such EEG alterations remain unclear. The authors evaluated the correlation between QEEG alterations that occurred during IFN-α treatment and the age of 98 patients with chronic hepatitis C. These patients underwent blind, prospective, and serial quantitative EEG examinations. IFN-α was administered intramuscularly at 9×10^6 IU daily for the first 4 weeks and then three times per week for the next 20 weeks. Serial EEGs were obtained before, at 2 and 4 weeks, and at 2 to 3 days after the treatment. The absolute powers of each frequency band at different stages of the treatment were determined by QEEG. The ages of the patients were classified into five groups: 20 to 29, 30 to 39, 40 to 49, 50 to 59, and ≥60 years. The relationship between the alterations in power values and age was statistically evaluated. As the age of the patients increased, the alterations in power values for the slow waves, alpha 2, and fast waves during IFN-α treatment became more remarkable, and significant (repeated-measure analysis of variance; $P < 0.0001$). The alterations of EEG occurring during IFN-α treatment were marked in older patients.

Key Words: Interferon-α, Quantitative EEG, Chronic hepatitis C, Age of patient.

(*J Clin Neurophysiol* 2005;22: 49–52)

Departments of *Neurology and ‡Neuropsychiatry, §Third Department of Internal Medicine, and ‖First Department of Internal Medicine, Nihon University Itabashi Hospital; Departments of †Neuropsychiatry and ¶Internal Medicine, Nihon University Surugadai Hospital; †Department of Internal Medicine, Itabashi Medical Association Hospital; and #Department of Hygiene and Public Health, Nihon University of Physical Education, Tokyo, Japan

This study was supported by a grant from the Ministry of Education, Culture, Sports, Science, and Technology for the promotion of the industry–university collaboration at Nihon University, Japan.

Address correspondence and reprint requests to Dr. Satoshi Kamei, Department of Neurology, Nihon University School of Medicine, 30–1 Oyaguchi-kamimachi, Itabashi-ku, Tokyo 173–8610, Japan; e-mail: skamei@med.nihon-u.ac.jp.

ISSN: 0736-0258/05/2201-0049

Alterations of brain waves on EEGs during treatment with interferon-α (IFN-α) have been described in several case reports (Meyers et al., 1991; Rohatiner et al., 1983; Smedley et al., 1983). We recently confirmed a diffuse slowing based on an analysis of blind, prospective, and serial quantitative-EEG (QEEG) examinations undertaken in many patients with IFN-α–treated chronic hepatitis C (Kamei et al., 1999). We speculated that such diffuse slowing on the EEGs could reflect a mild adverse effect on the brain caused by the IFN-α treatment. We also reported that this alteration of the quantitative EEG was clinically related to the change in score on the Mini-Mental State Examination (Kamei et al., 2002). However, no detailed investigations on clinical factors that may influence such EEG alterations during IFN-α treatment have yet been made. The present study is the first to evaluate the relationship between the alterations of quantitative EEG that occur during IFN-α treatment and the age of the patient.

SUBJECTS AND METHODS

Subjects

The subjects consisted of 98 previously reported patients with chronic hepatitis C who underwent our blind, prospective, and serial QEEG examinations (Kamei et al., 1999) during the period from August 1995 to May 2003. These patients were independently registered at three different hospitals (Nihon University Itabashi Hospital, Nihon University Surugadai Hospital, and Itabashi Medical Association Hospital) during this period. All patients had been investigated and treated under the same clinical regimen and conditions, including the diagnostic criteria, QEEG examinations, and IFN-α treatment, as reported previously (Kamei et al., 1999). The clinical diagnosis of chronic hepatitis C was confirmed on the basis of serologic findings of serum antibody for hepatitis C virus, histopathologic findings obtained by liver biopsy, detection of the viral genome sequence for hepatitis C virus by the reverse-transcriptase polymerase chain reaction, serum liver function tests, and the clinical course of the patients. IFN-α was administered intramuscu-